# Electron microscopy's multi-tool: the Scanning Transmission Electron Microscope

Vlad Stolojan
Advanced Technology Institute, University of Surrey, Guildford, UK.

**Biography:**
Vlad Stolojan obtained his BSc in Physics from University of East Anglia (1996) and his PhD in physics from University of Cambridge. After working at University of Cambridge on electron tomography, he moved to University of Surrey where he is currently and RCUK Research Fellow working on characterization of nano-electronic devices.

**Abstract:** A dedicated Scanning Transmission Electron Microscope is ideally coupled with the energy dispersive x-ray and electron energy loss spectroscopies to obtain information about the chemical composition, morphology and electronic structure on the nanoscale. With several signals being available simultaneously with the pass of a sub-nanometre-sized beam, this instrument can answer questions from a broad range of research areas, in a timely fashion. The user-friendliness of the instrument comes at almost no cost in performance, making it an ideal multi-tool in a teaching environment.

**Keywords:** STEM, EELS, EDX, Ronchigram

**Acknowledgements:** This work was partially supported by the EPSRC.

**Author Details:** Dr Vlad Stolojan
Advanced Technology Institute,
University of Surrey
Guildford GU2 7XH
UK
Tel: +44 1483 689411
Email: V.Stolojan@surrey.ac.uk

## Introduction

The majority of current scientific research is concerned with issues on the nanoscale, from adhesive joints in the aerospace industry to grain boundaries in metals and ceramics, from almost all aspects of nanotechnology to plasmonics and biology. Electron microscopy is able to provide structural, chemical and physical information on that scale through the variety of instruments and associated techniques available. Scanning Transmission Electron Microscopy combines some of the best characteristics of an SEM and a TEM. Similarly to an SEM, it forms a small probe which it then rasters across a sample to acquire spatial information from the surface-sensitive secondary electrons. However, the accelerating voltages are those of the TEM, so that various signals can be recorded in transmission, using the electrons that have passed through and interacted with the sample. Thus one can form SEM-like images with secondary electrons, to gain information about the surface of the sample, as well as TEM-like bright-field images (i.e. images formed with a parallel beam and an objective aperture

placed in the back-focal plane of the objective lens).The STEM is better than a simple sum of parts through a mode of imaging called Annular Dark Field (ADF) (Figure 1). This refers to images formed with the electrons that have interacted with and traversed the sample and have been recorded onto a 'donut-shaped' detector. When the angles are high enough (the 'donut' records scattering semi-angles from ~80mrad to ~260mrad), the image contrast is incoherent and is much more easily interpretable than that in bright-field TEM images, as the intensity depends linearly on the density, the thickness and the square of the atomic number of the specimen. One important thing to note here is that all three imaging modes (bright field, annular-dark-field and secondary-electron) can be acquired at the same time, within the same scan, the limitation being the number of video cards available in the instrument (usually two). The imaging information can also be further combined with spectroscopic information: energy-dispersive X-ray spectroscopy (EDX) and electron energy loss spectroscopy (EELS). EDX looks at the energies of the X rays generated by the incident electrons interacting inelastically with the sample, whilst EELS measures the energy lost by an incident electron through inelastic scattering. EDX offers chemical composition information for elements with medium to high atomic number, whilst EELS offers chemical composition for light elements and some of the transition metals, as well as electronic structure information, such as related to collective excitations (eg. plasmons), joint and local density-of-states. The spatial resolution of these techniques is related to the size of the electron probe itself (2.5Å to 10Å for an instrument without spherical aberration correction), as well as the size of the excitation event (eg. ~100Å when exciting a bulk plasmon, <0.5Å when exciting a single atom, ~10 to 30Å for X-rays). The STEM with EDX and EELS is an extremely powerful and versatile tool and this is reflected in the quality of results, with and without spherical aberration correctors [1-6].

**Materials and Methods**

In a wide research community, as found within a~~n~~ university, an investment in an expensive instrument, such as a transmission electron microscope, has two major requirements: the first is that it provides competitive information across a broad range of fields of study and the second is that, as an instrument in a teaching environment, its' user-friendliness allows students to divert more attention to the science(i.e. their sample) within the instrument and the science behind the instrument, so that it becomes a true multi-user microscope. The STEM is a natural choice for users that want to combine classical electron microscopy with analytical spectroscopic studies on the nanoscale. At the University of Surrey, this ~~is~~ role is performed by the Hitachi HD2300A STEM with a Schottky field-emitter, which can be operated at 200 and 120keV accelerating voltages. The instrument is fitted with a Gatan Enfina EEL Spectrometer and an EDAX EDX spectrometer (figure2). The instrument consists of a pair of condenser lenses for forming the probe, an objective lens for focusing and a projector lens for changing the solid angles into the various detectors in normal imaging mode and for changing the camera length in diffraction mode. The instrument has four main operating modes, effectively equivalent to four different probe sizes, from 10Å down to 2.5Å called EDX, Normal, High Resolution and UltraHighResolution. There are also two extra modes, one is diffraction and the other is DECON(tamination). In the DECON mode, a broad beam is rastered across a region of interest of the sample to burn off any of the volatile carbon radicals

present on the surface of the sample, which harden into a carbon deposit as the electrons are formed into a very small and intense spot.

One important difference from TEMs here that the magnification is realized through the way the sample is scanned, much like an SEM, as opposed to using several projector lenses. This has the great advantage that, once an operating mode is selected, the lens currents stay virtually constant. The disadvantage is that, at low magnifications (<100k), the electron beam is scanned sufficiently far from the centre of the objective lens to be affected by the spherical aberration of the lens and also to affect the collection of energy loss spectra whilst the beam is scanned.

One of the biggest advantages in operating the STEM is the Ronchigram, the shadow image of the stationary probe going through the sample and projected onto a CCD camera. The Ronchigram makes alignment, stigmation and focusing intuitive, as well as making the measurement of aberrations relatively straightforward [7]. It is no surprise that the Ronchigram underpins the success of the Nion spherical aberration corrector [8] and the Nion SuperSTEM II [9]. It is also the basis of the 'aperture less' microscopy recently proposed [10]. Furthermore, it is an excellent way to teach new users about electron microscopes, as it is a true 'one-stop' shop for their alignment [7]

**Examples**

Biological specimens are a particular case where the STEM can provide essentially unrivalled information through the mass-thickness and $Z^2$ contrast present in High-Angle ADF images. The image of a DNA molecule supported on a carbon film revealed the power of this instrument as long ago as 1971 [11]. Beam damage is reduced significantly as a result of scanning rapidly the intense probe across the sample, thus reducing the overall damage. The Ronchigram serves to focus on the sample very quickly and easily, even during the acquisition of an image. Figure 3a shows a HAADF image of a cancer cell infected with reo-viruses and Figure 3b its equivalent bright field image, one that would be obtained using a TEM (for comparison purposes, we have used the PL in our STEM to increase the acceptance angle into the bright field detector, so as to reproduce TEM conditions as closely as possible). It is worth noting that these images were collected at what are very harsh conditions for biological samples: room-temperature specimen holder, 200keV accelerating voltage. Without the Ronchigram, these images would have probably been nearly impossible to achieve. These images show that the cancer cell has been successfully infected with reo-viruses, which arrange in clusters distributed throughout the cell's body. The inset in Figure 3a shows a close-up of a virus, with its' characteristic hexagonal head.

The simultaneous availability of the SE, BF and HAADF/ADF signals is advantageous when studying carbon nanotubes, particularly when they are embedded in polymers (figure 4). Due to the different secondary electron **cross-sections** for carbon nanotubes and polymers, the carbon nanotubes are readily visible in the SE image, compared to BF and ADF images, as they are the virtually the same material (i.e. carbon). The simultaneous availability of these signals makes the imaging and the analysis of embedded carbon nanotubes a more straightforward exercise, with added information about the surface morphology and/or the contamination of these nanostructures.

The difference between incoherent and coherent imaging can be seen in Figure 5, where 5a) is the HAADF image of a $WS_2$ nanotube (the lattice planes are separated by 6.2Å) and the simultaneously acquired bright field image. In the bright field image (Fig. 5b), the position of the W planes is unclear as the position and contrast of the fringes (bright or dark) depends on the defocus, whilst the contrast in the HAADF image is mainly $\alpha$ $Z^2$.

The last example presented here is a detailed examination of amorphous Si implanted with Mn using ion beam implantation ( energy, dose) and annealed using an excimer pulsed laser (energy, dose), with the goal of forming small magnetic Mn clusters. Manganese can also form three variants of the silicide: non-magnetic SiMn, antiferromagnetic $Mn_5Si_3$ and magnetic $Mn_4Si_7$. The HAADF image in figure 6a shows that the implanted region is crystallized, with Si crystallites ~30nm in diameter, with increased intensity in the grain boundary region. The increased intensity at the grain boundaries could be caused by densification as well as an increase in the Mn concentration at the boundaries. EDX mapping (not shown here) confirms that Mn does indeed migrate to grain boundaries and is confined to the crystallized region, as predicted from the binary phase diagram. EELS mapping along the green line in figure 6a shows the relative distribution of Mn confined to the crystallized region, as extracted from the area under the Mn white line. The Mn white line represents the spectral feature associated with energy lost by the incident electrons to Mn atomic transitions from the spin-orbit split 2p energy level to empty states in the 3d band (called 'white lines' because that is how they appeared on the original photographic recordings of energy loss spectra). Figure 6c shows a trace of the relative Mn composition across a grain boundary, taken with steps of 7Å, showing a Mn-rich region of ~5nm width. This allows us to switch our STEM into nano-diffraction mode and collect a diffraction pattern from a region ~3nm at the grain boundary (Figure 6d). Comparing the diffraction data with that from the manganese silicides [12-14], we conclude that the spots marked by the red circle in 6d are due to 220 planes in the antiferromagnetic $Mn_5Si_3$.

## Conclusion

Scanning Transmission Electron Microscopy is the ideal operating mode when probing the chemical, compositional and electronic structure information on the nanoscale with spectroscopic and imaging techniques. At the University of Surrey, we have opted for a dedicated STEM instrument with EDX and EEL spectrometers for providing in-depth information on the nanoscale for a wide range of samples, characteristic of the broad research efforts usually associated with an university: from biology to materials science, from nanostructures to interfaces. We found the SEM-like user-friendliness of our instrument particularly attractive to student users and the simultaneous availability of several imaging and spectroscopic signals very useful in answering questions about the science and processes related to samples in a timely fashion. Although STEM as an instrument has always had a niche following, the quality of the results obtained in the last two decades justify it as a stand-alone instrument.

## References


[1] Muller, D. A. et al. *The electronic structure at the atomic scale of ultrathin gate oxides.* Nature 399: 758-761, 1999.

[2] Muller, D. A. et al. *Atomic-scale chemical imaging of composition and bonding by aberration-corrected microscopy*. Science 319: 1073-1076, 2008.

[3] Nellist, P. D. et al. *Direct imaging of the atomic configuration of ultradispersed catalysts.* Science 274: 413-415, 1996.

[4] Nellist, P. D. et al. *Direct sub-angstrom imaging of a crystal lattice*. Science 305: 1741-1741, 2004.

[5] Li, Z. Y. et al. *Three-dimensional atomic-scale structure of size-selected gold nanoclusters.* Nature 451: 46-48, 2008.

[6] Nelayah, J. et al. *Mapping surface plasmons on a single metallic nanoparticle*. Nature Physics 3: 348-353, 2007.

[7] The Ronchgram: http://www.rodenburg.org/STEM/t200.html.

[8] The spherical aberration corrector: http://www.nion.com/tech.html.

[9] The Daresbury Laboratory SuperSTEM facility: http://www.superstem.dl.ac.uk.

[10] Rodenburg, J. M. et al. *Transmission microscopy without lenses for objects of unlimited size.* Ultramicroscopy 107: 227-231, 2007.

[11] Crewe, A. V. et al. Visibility of a single atom. Science 168: 1338-1340., 1970.

[12] Gottlieb, U. et al. *Magnetic properties of single crystalline Mn4 Si7*. J. Alloys Compd. 361: 13-18, 2003.

[13] Jorgensen, J.E. and Rasmussen, S.E. *Refinement of the structure of MnSi by powder diffraction*. Powder Diffraction 6: 194-195, 1991.

[14] Brown, P.J. and Forsyth, J.B. *Antiferromagnetism in Mn5 Si3: the magnetic structure of the A F2 phase at 70K*. J. of Phys.: Cond. Matter 7: 7619-7628, 1995.

**Figure 1**

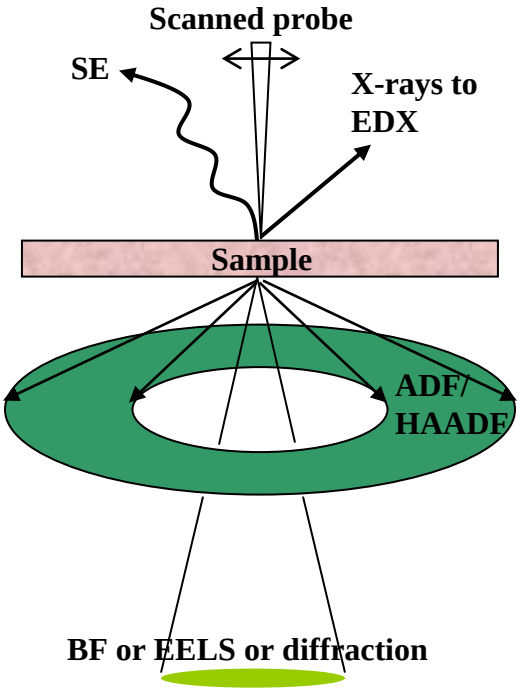


**Figure 1:** Schematic diagram of the signals available in the STEM. The secondary electrons (SE) and the X-rays generated by the scanned probe are collected at detectors above the sample, whilst the annular dark field (ADF or HAADF, depending on the angle range) and the bright field (BF) are collected below the sample. EELS, diffraction and the bright field signal are mutually exclusive, as they involve the same scattered electrons.

**Figure 2**

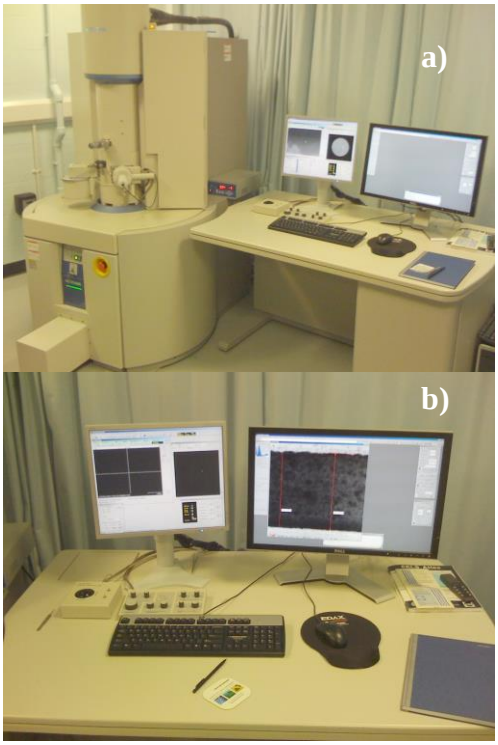


**Figure 2 a)** The Hitachi HD2300A STEM at University of Surrey. Fitted with an EDAX EDX spectrometer and an Gatan Enfina EELS spectrometer. **b)** Detail of the control console, showing two LCDs: the left-hand-side one is for controlling the microscope and the right-hand-side one is used interchangeably between the two spectrometers. The operation of the STEM is very much in Hitachi SEMs function, with an extremely simple 'buttons' box and a separate stage control unit.

**Figure 3**

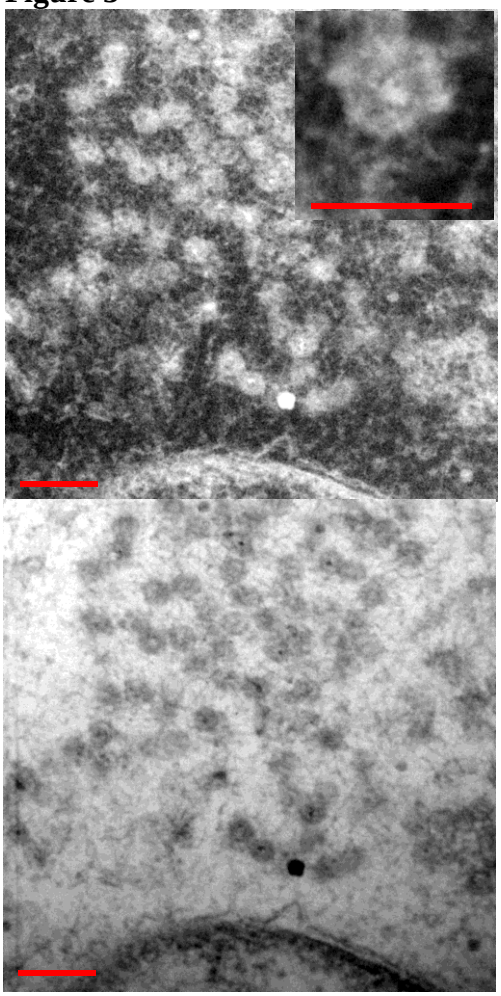

**Figure 3 a)** HAADF image of a cluster of reo-viruses that have infected a cell from a mouse's skin melanoma. The inset shows a typical reo-virus, with its characteristic hexagonal body. **b)** Equivalent bright-field image of the cluster of the reo-viruses. The contrast in this image is affected by interfence (coherent contrast), which makes interpretation more difficult. Sample courtesy of Dr Lucy Heinemann, University of Surrey.

**Figure 4**

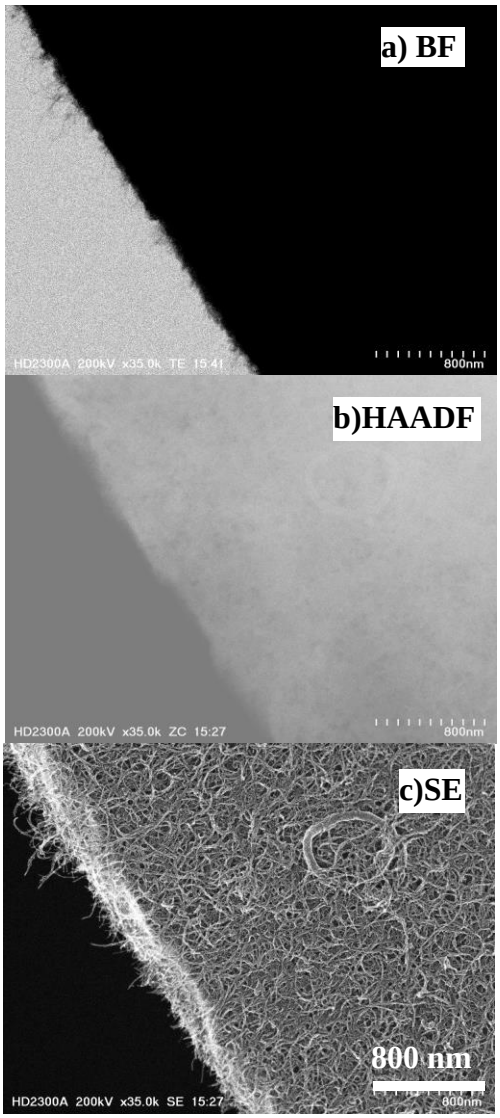


**Figure 4**. Low magnification images of carbon nanotubes dispersed in PPV (poly-..). Secondary electrons are generated preferentially in the carbon nanotubes. The thickness of the sample affects significantly the bright-field image (a), so only nanotubes at the edge of the sample are visible. The HAADF image (b) shows that the thickness and density of the film are uniform, whilst the SE image (c) shows the location and distribution of carbon nanotubes within the polymer. Sample courtesy of Dr Ross Hatton, University of Surrey.

**Figure 5**

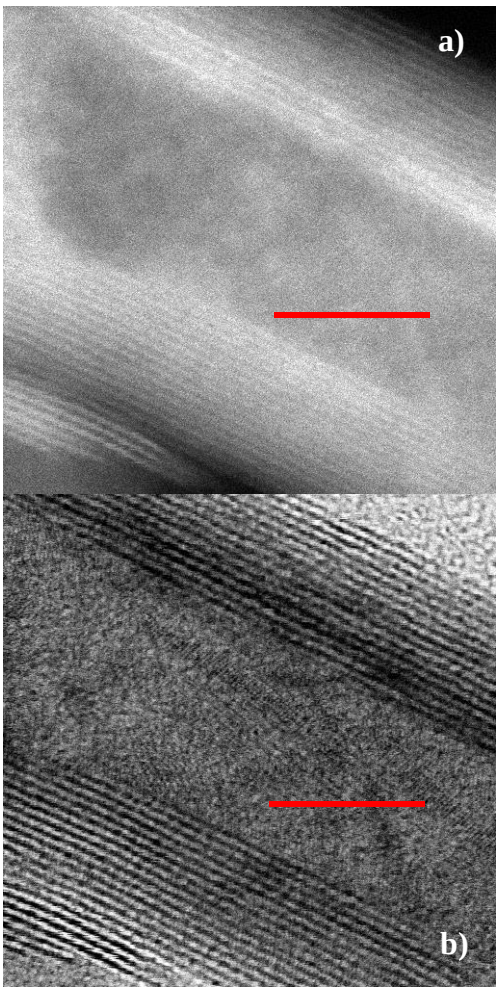


**Figure 5 a)** HAADF image of a $WS_2$ nanotube showing the position of the W concentric shells (the repeat unit is –S-W-S-, with two layers of S atoms between the W atoms). **b)**The equivalent bright field image is more difficult to interpret due to the coherent contrast effects. Sample courtesy of Dr Jeremy Sloan, University of Surrey and Queen Mary's College London.

**Figure 6**

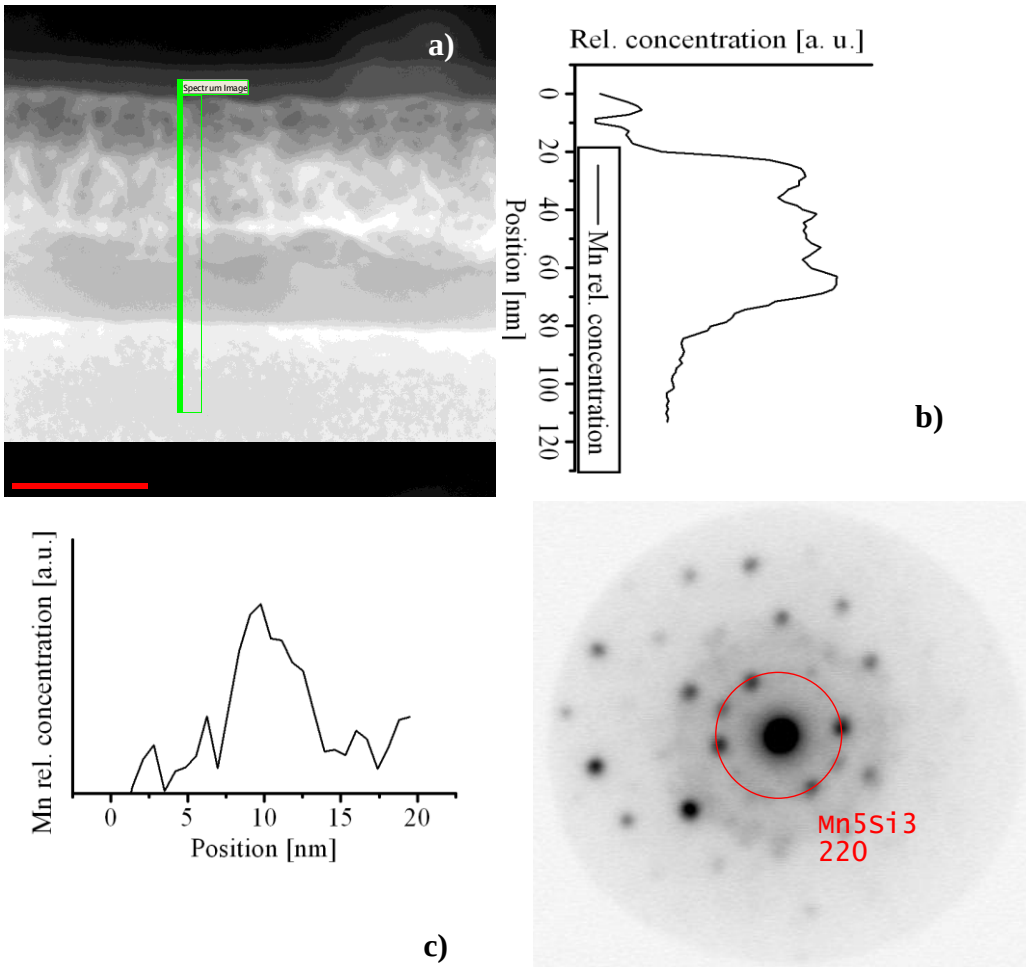


**Figure 6 a)** An HAADF image of an amorphous Si layer deposited on a Si substrate which has been ion-beam-implanted with Mn and annealed with a pulsed excimer laser. Upon annealing, the amorphous Si crystallizes in grains ~30nm in diameter and the Mn migrates to the grain boundaries. **b)** EELS acquired at positions along the green line reveals that Mn is distributed in the crystallized layer. The plot has been oriented so that the spatial dimension corresponds to that in the image in panel a). **c)** a detailed profile collected across the boundary confirms that Mn decorates the grain boundaries, in a region ~6nm thick. **d)** This allows us to collect diffraction patterns with a small, ~3nm diameter probe from the region and show that the Mn does not form the non-magnetic MnSi. Sample courtesy of Dr Nianhua Penh, University of Surrey.